

Validation and determination of ice water content-radar reflectivity relationships during CRYSTAL-FACE: Flight requirements for future comparisons

D. S. Sayres,¹ J. B. Smith,¹ J. V. Pittman,^{1,2} E. M. Weinstock,¹ J. G. Anderson,¹ G. Heymsfield,³ L. Li,⁴ A. M. Fridlind,⁵ and A. S. Ackerman⁵

Received 18 April 2007; revised 18 October 2007; accepted 26 November 2007; published 6 March 2008.

[1] In situ measurements of cirrus ice water content (IWC) by the Harvard water vapor and total water instruments during Cirrus Regional Study of Tropical Anvils and Cirrus Layers-Florida Area Cirrus Experiment are compared with remote sensing data made by the Cloud Radar System instrument in order to derive and validate an empirical IWC-radar reflectivity Z_e relationship. The comparisons show that for measurements of in situ IWC and remotely measured radar reflectivity, collocated within 2 km of each other, a single IWC- Z_e relationship can be found that fits the data with an uncertainty of ± 20 –30%. A cloud resolving model shows this level of uncertainty to be consistent with sampling errors associated with comparing two measurements that are not collocated. Uncertainties are quantified in the use of in situ data to validate the retrieval algorithms used to derive the IWC of clouds from remote sensing observations, such as radar reflectivity Z_e . Uncertainties are classified into instrumental uncertainties, uncertainties related to sampling errors, and uncertainties in using a single IWC- Z_e relationship to describe a cloud.

Citation: Sayres, D. S., J. B. Smith, J. V. Pittman, E. M. Weinstock, J. G. Anderson, G. Heymsfield, L. Li, A. M. Fridlind, and A. S. Ackerman (2008), Validation and determination of ice water content-radar reflectivity relationships during CRYSTAL-FACE: Flight requirements for future comparisons, *J. Geophys. Res.*, 113, D05208, doi:10.1029/2007JD008847.

1. Introduction

[2] Clouds play a critical role in determining the radiative budget of the atmosphere and surface by the absorption and scattering of solar and terrestrial radiation [Norris, 2000]. The extent to which clouds scatter and absorb radiation is determined by the microphysical and geometric structure of the cloud [Baran, 2005]. In order for clouds to be represented more accurately in general circulation models (GCMs) the vertical structure of ice water content (IWC), particle size distribution, and particle geometry (habit) in clouds needs to be obtained on a global scale [Stephens *et al.*, 2002]. Accurately representing clouds in GCMs and climate models is paramount for enabling models to predict how changes in emissions of pollutants will affect cloud formation and evolution, upper tropospheric water vapor, and the radiative budget of the atmosphere. However, to

date cloud processes represent one of the largest uncertainties in GCMs [Stephens, 2005].

[3] In order to improve our understanding of cloud physics several measurement campaigns using balloon and aircraft in situ measurements have been devoted to studying the microphysical and macrophysical properties of clouds [Pawlowska *et al.*, 2000; Gultepe *et al.*, 2001; Buschmann *et al.*, 2002; Nasiri *et al.*, 2002; and references therein]. While in situ measurements provide high spatial resolution, they typically provide only a one-dimensional (1-D) trajectory through a cloud and within the limit of aircraft flight time can only sample a small fraction of a cloud. In recent years, remote sensing probes such as radar and lidar have become central to the effort to quantitatively measure microphysical properties of clouds on a large scale. The culmination of this effort is NASA's launch of a suite of satellites known as the A-Train [Stephens *et al.*, 2002]. The A-Train consists of six satellites flying in formation so that all make observations of the same volume of atmosphere within 15 min of each other. CloudSat, a 94 GHz cloud-profiling radar, and CALIPSO, a two channel (532 and 1064 nm) cloud and aerosol lidar, are focused on making high-resolution measurements of the microphysical properties of clouds such as IWC, median ice particle volume diameter, and particle shape.

[4] The physical properties of clouds are deduced by remote sensing instruments from the scattering of radar and lidar signals or by their infrared emission. Radar

¹Department of Earth and Planetary Sciences, Harvard University, Cambridge, Massachusetts, USA.

²Marshall Space Flight Center, NASA, Huntsville, Alabama, USA.

³Goddard Space Flight Center, NASA, Greenbelt, Maryland, USA.

⁴University of Maryland, Baltimore County, Baltimore, Maryland, USA.

⁵NASA Goddard Institute for Space Studies, New York, New York, USA.

instruments measure the reflectivity from cloud particles caused by the angular dependence of scattering of the radar beam. The radar reflectivity Z_e can be related to the IWC of the cloud via a power law relationship detailed in section 2. Since different clouds and regions within a cloud possess different particle-size distributions, habits, and ice densities, a suite of relationships, each set representing a particular category of cloud, is required to describe an ensemble of cloud types. To determine which relationship to use for a particular cloud and to minimize the uncertainty in the IWC- Z_e relationships, several approaches have been suggested using the extinction coefficient from lidar [Wang and Sassen, 2002a, 2002b], the mean Doppler velocity [Donovan, 2003], or cloud top temperature [Liu and Illingworth, 2000]. However, given the ability to categorize clouds on the basis of remote measurements, great importance still must be placed on obtaining and validating coefficients for each cloud type.

[5] The first step in deriving IWC- Z_e relationships for different clouds is to obtain IWC and the corresponding Z_e . Previous comparisons have used in situ particle size data [Brown and Illingworth, 1995; Liu and Illingworth, 2000] or modeled size spectra of pure hexagonal columns and plates to derive IWC and Z_e [Aydin and Tang, 1997; Sassen et al., 2002]. These studies have reported uncertainties in the derived IWC of as much as 60% for a given value of Z_e . For the comparison presented here we use direct measurements of in situ IWC and remotely detected radar reflectivity obtained during the Cirrus Regional Study of Tropical Anvils and Cirrus Layers-Florida Area Cirrus Experiment (CRYSTAL-FACE) [Jensen et al., 2004].

[6] The interpretation of this comparison is complicated by the spatial and temporal differences between the air parcels that the in situ and remote instruments measure. To address the uncertainties inherent in comparing IWC from in situ and remote measurements, we group the uncertainties into three categories not only to best constrain the parameters that are needed to derive IWC from Z_e but also to try to determine the most efficient way to carry out these validation experiments.

[7] 1. Instrumental uncertainties in the measurement of IWC and radar reflectivity. These uncertainties are assumed to be fixed for a given comparison and independent of the cloud being measured.

[8] 2. Uncertainty in matching in situ data with remote data, which we refer to as sampling error. This error occurs because of the reality that there is often spatial or temporal separation between the in situ measurement and the remote measurement. Because of the large variability of IWC or cloud inhomogeneities, measurements that are not collocated can lead to erroneous (noninstrumental) errors in the comparison.

[9] 3. Uncertainty in the relationships used to calculate IWC from Z_e . This uncertainty includes the sensitivity of the constants used in this calculation to variations in habit, size distribution, and ice density. This category also includes estimates of the uncertainty resulting from cloud-type variability.

[10] Instrumental uncertainties and the error in derived IWC are discussed in section 3.1. Section 3.2 discusses the comparisons made during the CRYSTAL-FACE mission and the uncertainty associated with using different IWC- Z_e

relationships. Section 4 uses a cloud model to evaluate the error associated with insufficient overlap between two instrument measurements.

2. Physical Basis for the IWC- Z_e Relationship

[11] The magnitude of the radar reflectivity Z_e , due to Rayleigh scattering, is proportional to $\int n(D)D^6 dD$, where n is the number density of particles with diameter D [Liao and Sassen, 1994]. However, this is only valid for small spheroidal particles and does not account for Mie scattering or the effect of particle shape and density. Equation (1) is a modified form of this relationship proposed by Liu and Illingworth [2000], where a term accounting for particle shape has been added,

$$Z = \int n(D)D^6 K(m, \rho)^2 f(D, \rho) h(D, \rho) / 0.93 dD, \quad (1)$$

where K is a factor dependent on the refractive index of ice m , f is the ratio of Mie to Rayleigh scattering, h is a shape factor dependent upon the habit of the particles, and the factor 0.93 is chosen so that for liquid water the relationship reduces to the equation for spheroidal droplets.

[12] IWC, defined as the mass of ice per unit volume of air, can be written as

$$IWC = \int \rho V n(D) dD, \quad (2)$$

where n is the number density of particles with volume V and mass density ρ . By inspection of equations (1) and (2), Z is proportional to the square of IWC. However, the power dependence on the particle diameter in equations (1) and (2) assumes spheres with constant density. For real cirrus particles the relationship is not a perfect square. The relationship between IWC and Z_e , the equivalent reflectivity for ice, can thus be written as a power law

$$IWC = aZ_e^b, \quad (3)$$

where IWC is measured in g/m^3 , Z_e is measured in mm^6m^{-3} , and a and b are functions of particle size distribution, habit, and ice density. Given measurements of IWC and corresponding Z_e values, the coefficients a and b are determined empirically by regression of IWC with Z_e .

3. Direct Comparisons of In Situ IWC and Remote Z_e Data

[13] The CRYSTAL-FACE campaign took place out of Key West, Florida, during July 2002. The main focus of the mission was to study the physical properties of subtropical cirrus clouds in order to improve our understanding of the formation and evolution of cirrus and to improve our ability to model cirrus in GCMs. In order to accomplish this objective several aircraft were used, each carrying a different suite of instruments and each measuring a different level of the atmosphere. Another goal of CRYSTAL-FACE was to compare and validate remote sensing instruments flown on the ER-2 with in situ measurements from the WB-57. The ER-2 carried remote sensing instruments similar to

those that are part of the A-Train constellation of satellites. The Cloud Radar System (CRS) and Cloud Physics Lidar (CPL) have similar capabilities to the instruments aboard the CloudSat and Cloud-Aerosol Lidar and Infrared Pathfinder Satellite Observation satellites, respectively. The WB-57 carried a suite of in situ instruments measuring IWC (Harvard total water and water vapor), particle size distributions, habit, and aerosols, as well as tracer and meteorological measurements.

3.1. Flight Plans and Instruments

[14] An example of coordinated flight segments used to compare remote and in situ IWC measurements took place during the flight of 16 July. The ER-2 made several passes over a convective system that developed over Florida and moved westward, while the WB-57 made several passes through the cirrus outflow of the same convective system. This makes the flight of 16 July ideal for comparing remote and in situ data. While during other flights the ER-2 and WB-57 flew together, they were sampling several different clouds and therefore did not sample air parcels close enough in time and space to make reasonable comparisons. For the purpose of this comparison we focus on IWC retrieved from radar and measured in situ. While more accurate IWC retrievals can be derived from combining multiple remote measurements, such as radar and lidar, the CPL lidar did not report data for the 16 July flight. Since most of the comparisons presented in this paper are from 16 July, the simpler IWC- Z_e relationship was chosen. Radar reflectivity was measured using the CRS instrument that flew aboard the ER-2 aircraft and IWC was measured using the Harvard Lyman α total water (HVTW) and water vapor hygrometers aboard the WB-57.

[15] The CRS instrument is a 94 GHz Doppler polarimetric radar mounted in the right wing pod of the ER-2 [Li *et al.*, 2004]. The 94 GHz frequency allows CRS to measure a wide range of clouds, from thin cirrus to thick convective anvils. The units of reflectivity (Z_e) are mm^6m^{-3} . However, Z_e is often reported in units of power (dB), where $1\text{ dBZ}_e = 10\log_{10}(\text{mm}^6\text{m}^{-3})$. The sensitivity of the CRS instrument is -29 dBZ_e at 10-km range, 150-m resolution, and 1-s averages. To maintain the calibration of the radar, average transmit power and receiver gain are continuously monitored in order to have in-flight diagnostics as to the transmitter stability. In addition, external calibration against other radar systems yields an uncertainty of 1 dB. The spatial resolution of the reflectivity data reported by the CRS instrument for the CRYSTAL-FACE mission is 1 km horizontally and 75 meters vertically along the flight path of the ER-2. A retrieval algorithm using Brown and Illingworth's [1995] relationship was used to calculate the archived remote IWC data. The coefficients used for the retrieval are derived from ice crystal size spectra from a 2-D optical array probe sampling cirrus from midlatitude frontal systems. The size spectra are converted to IWC and radar reflectivities via equations similar to equations (2) and (1), respectively. For the IWC the bulk density is assumed to be proportional to $D^{-1.1}$, where D is the mean volume diameter of the particles. A simple least squares fit to equation (3) yields the parameters a and b . The CRS data use a K^2 value of 0.695 which is appropriate at 94 GHz under 0°C conditions. However, previous measurements have used

K^2 equal to 0.93 in order that the reflectivities be scaled to liquid water. In order to compare the data presented here with previous measurements we have rescaled the CRS data by subtracting 1.26 dB.

[16] HVTW measures total water (i.e., vapor plus ice) directly. IWC is derived by subtracting water vapor, as measured by the Harvard water vapor instrument, from total water. Both Harvard water vapor and total water measure water vapor by using Lyman α to photodissociate water into an OH fragment in its first excited electronic state. The excited OH fragment then either relaxes via fluorescence or is quenched during a collision with an air molecule. Within the range of ambient densities encountered during CRYSTAL-FACE the magnitude of the fluorescence signal is directly proportional to the mixing ratio of water.

[17] Calibrations are performed at a range of pressures and water vapor mixing ratios [Weinstock *et al.*, 2006b]. Water vapor is injected into the calibration system using a bubbler and checked via long-path and short-path (axial) absorption. The calibration is therefore tied to two fundamental standards: the vapor pressure of water over liquid at room temperature and the absorption cross section of water vapor at the Lyman α wavelength. In-flight validation consists of cross checking changes in the ambient water vapor mixing ratio (i.e., $\Delta\text{H}_2\text{O}$) using both dual-path (axial) absorption and fluorescence. In addition, in clear air the total water instrument is compared to the water vapor instrument. Agreement between the two instruments increases confidence in the water vapor measurement and the IWC product [Weinstock *et al.*, 2006a].

[18] During flight operation the HVTW instrument uses a roots pump downstream of the detection axis to pull ice particles and water vapor into the instrument duct, while maintaining isokinetic flow to ensure that the number density of particles entering the inlet is the same as the ambient number density. A 600-W inlet heater evaporates the ice particles and the total water is measured. The precision of the total water instrument is 5% and the accuracy with respect to ice water content is 15% [Weinstock *et al.*, 2006b]. Agreement with other in situ IWC measurements is better than 20% for IWC greater than 0.01 g/m^3 [Davis *et al.*, 2007]. The minimum detectable IWC for the CRYSTAL-FACE mission is $1 \times 10^{-4}\text{ g/m}^3$. HVTW uses a 1-s integration time and because of the speed of the aircraft this yields a horizontal resolution of 100–200 m. For the purposes of this comparison, 10-s data, which produces 1.5-km averages, are used in order to make the horizontal resolution consistent with that of the CRS instrument.

3.2. Direct Comparison of Data

[19] If both the ER-2 and WB-57 were coordinated so that the instruments were always sampling the same footprint at the same time, then a direct comparison between the instruments would be straightforward. However, because of constraints on aircraft velocities and air traffic control most of the time the instruments will not be sampling the same air parcel. Instead, there will be some finite distance and time between when the cloud is sampled by the in situ instrument and the cloud is sampled by the remote sensing instrument. It is therefore imperative that these spatial and temporal differences be taken into account and ideally minimized when making the comparison. We first address the temporal

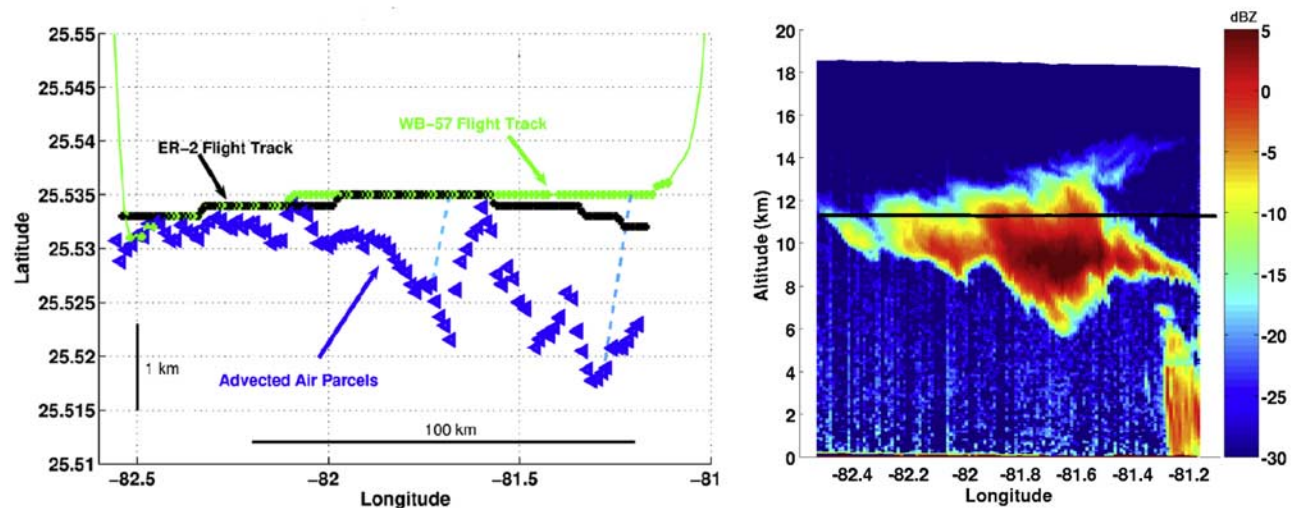


Figure 1. (left) Advection of air parcels between when the ER-2 and WB-57 sampled the same region. The black points represent the ER-2 flight track, the green points represent the WB-57 flight track, and the blue triangles correspond to the air parcels sampled by the WB-57 advected back to where they would have been when the ER-2 sampled this region. The light blue dashed lines show the advection of selected air parcels during the time lag between the ER-2 and WB-57. Note that the x and y axes have different scales as indicated by the black scale lines in the figure. (right) The radar reflectivity from the CRS instrument and the altitude of the WB-57 plotted in black.

difference between when the ER-2 and WB-57 sample a region by making a first-order correction for the movement of air parcels using the wind velocity measured aboard the WB-57 by the Meteorological Measurement System (MMS). A detailed description of the derivation of wind velocity from MMS measurements is given by *Scott et al.* [1990].

[20] The flight of 16 July represented the best day for doing direct comparisons. Two views of a flight segment from 16 July are shown in Figure 1. An overhead view is shown on the left-hand side with the flight tracks of the WB-57 and ER-2 plotted in green and black, respectively. The right-hand plot shows a vertical view, with the reflectivity from the CRS instrument shown in colors according to the legend and the altitude of the WB-57 plotted as a black line. The ER-2 took approximately 10 min to traverse the cloud and the WB-57 lagged the ER-2 by between 2 and 8 min. For each time interval that data are reported along the ER-2 flight track the air parcels sampled by the WB-57 are advected back to where they would have been at the time the CRS instrument made a measurement. The air parcel sampled by the HVTW instrument that is nearest to the air parcel sampled by the CRS instrument is then used in the comparison. The result is shown in Figure 1 (left), where the blue triangles correspond to the air parcels sampled by the WB-57 advected by the winds measured along the WB-57 flight track during the time lag between the ER-2 and WB-57 cloud encounter. As is evident in the figure, even within a few minutes there can be considerable movement of air parcels.

[21] Figure 2 shows the in situ HVTW and retrieved CRS IWC plotted versus time along the ER-2 flight track in black and gray, respectively. The CRS IWC is the archived data using *Brown and Illingworth's* [1995] algorithm. The left-

hand plot shows data taken during a flight transect through a cloud on 16 July between 2206 and 2216 UT (this is the same transect shown in Figure 1). The colored points on the bottom of the plot show the horizontal distance between the air parcels sampled by HVTW and CRS with dark blue being points separated by a few 100 m and red being points separated by more than 3 km. The horizontal separation distance is the distance after the air parcels sampled by HVTW have been advected as described earlier. For the data shown in the left plot of Figure 2, the distance between the air parcels being sampled ranges from a few 100 m to 2 km. For this comparison the retrieved IWC agrees with the in situ IWC to within 20% and, in general, reproduces the structure of IWC in the cloud.

[22] If we now look at a case where the sampled air parcels are 5 km away from each other (right plot of Figure 2), the two measurements do not agree because, while the strength and direction of the wind have been accounted for, the IWC in a cloud varies significantly in magnitude and structure even over a few km. This is evident in several other examples where the measurements agree fairly well when the air parcels being sampled are within 2 km and the comparison breaks down as the distance between the parcels becomes greater than 2 km. This is consistent with the modeled sampling error caused by inadequate spatial overlap discussed in section 4. The maximum acceptable distance for a reasonable comparison will depend on the level of cloud inhomogeneities, with 2 km being the distance associated with the clouds sampled during CRYSTAL-FACE. By limiting the comparison to flight legs where both the ER-2 and WB-57 were within 2 km of each other the error caused by insufficient spatial overlap should be small at least for clouds with comparable inhomogeneities. During the month long CRYSTAL-FACE mission, there were only eight flight

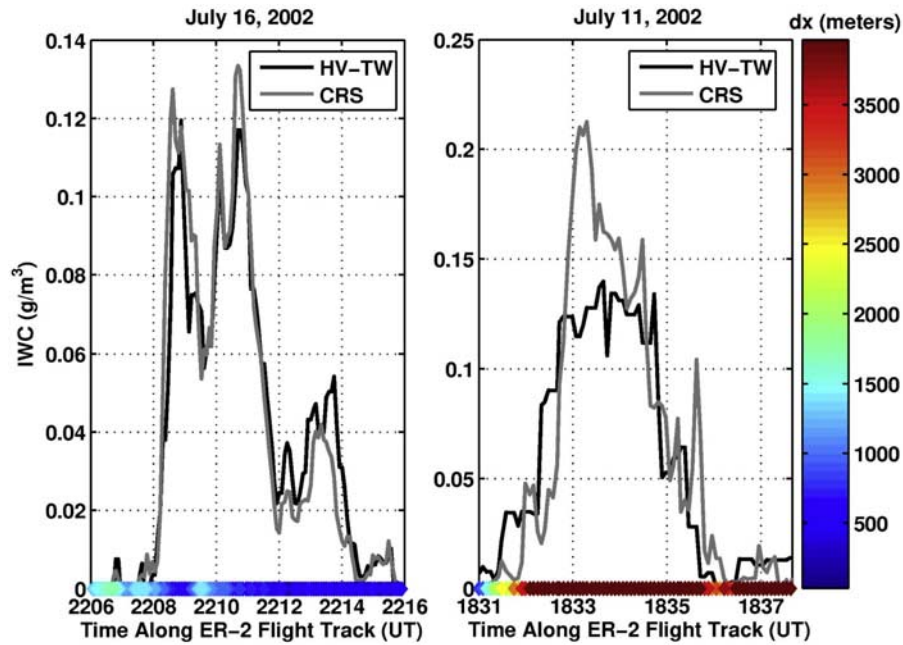


Figure 2. Comparison of IWC measured in situ by HVTW and derived remotely by CRS, during a cloud transect on (left) 16 July at 2206 UT and (right) 11 July at 1831 UT. HVTW is plotted in black and CRS is plotted in gray versus time along the ER-2 flight track. The colored points along the bottom of the plots represent the horizontal distance between the air parcels sampled by both instruments. The color code is given by the vertical colorbar.

legs where both aircraft sampled clouds within 2 km of each other. This results in only 37 min of data out of approximately 70 h of flight time.

[23] The comparisons shown in Figure 2 use IWC derived from Z_e using *Brown and Illingworth's* [1995] relationship. However, the parameters in this relationship were derived from tropical cirrus clouds and are possibly not appropriate for the anvil cirrus sampled during CRYSTAL-FACE. In order to determine which IWC- Z_e relationship best fits the CRYSTAL-FACE data a linear least squares fit to equation (4) is performed to derive the coefficients a and b for each flight leg where data from HVTW and CRS are within 2 km. We convert equation (3) from mm^6m^{-3} because CRS reports Z_e in terms of dBZ_e . This results in the linear equation,

$$\log_{10}(\text{IWC}) = \log_{10}(a) + \frac{b}{10}Z_e. \quad (4)$$

[24] The data are fit by minimizing the weighted residuals in both variables. The data are weighted using a 1 dB uncertainty in radar reflectivity and a 15% uncertainty in IWC. Shown in Figure 3 are scatter plots of $\log_{10}(\text{IWC})$ versus Z_e for data that are within 2 km of each other along with regression lines using different parameters for a and b . In Figure 3a each of the flight legs is plotted as a different symbol as indicated by the figure legend and shaded by temperature as given by the colorbar in the figure. Also shown are IWC- Z_e relationships using the coefficients of *Protat et al.* [2007] which are given as a function of temperature. Shown in the figure are lines for -70 , -60 , -50 , and -40°C from left to right. A small trend in the IWC- Z_e relationship with temperature is noticeable in the

data, especially at larger IWC. However, there is considerable scatter in the data as a function of temperature. For this data set a single best fit line can be found that fits the data to within $\pm 20\%$ ($2-\sigma$) for IWC greater than 0.05 g/m^3 and to within $\pm 40\%$ for IWC less than 0.05 g/m^3 . The least squares fit to all the data is shown in Figure 3b as a black, thick-dashed line. Also shown are the IWC- Z_e relationships using the coefficients of *Liu and Illingworth* [2000], *Brown and Illingworth* [1995], and *Aydin and Tang* [1997] as gray lines given by the legend. The coefficients derived from this work as well as those from previous comparisons are listed in Table 1. Table 1 also includes characterizations of the clouds used in each study.

[25] Figures 4 and 5 show the eight comparisons that were made during CRYSTAL-FACE. The comparisons are divided by cloud thickness, with thinner cirrus plotted in the top four plots and thicker cirrus plotted in the bottom four plots. For each comparison plot in Figure 4 the in situ IWC data from the HVTW instrument are plotted in black and the derived IWC data using the fit coefficients from this work are plotted in blue. Also shown are derived IWC data using the relationships described by *Brown and Illingworth* [1995], *Liu and Illingworth* [2000], *Protat et al.* [2007], and *Aydin and Tang* [1997] in purple, magenta, cyan, and red, respectively. For each comparison plot in Figure 5 the data are plotted as the fractional difference between the in situ IWC data from HVTW and the derived IWC data. The colors are the same as in Figure 4. For three of the four thin cirrus cases (Figures 4a, 4c, 4d, 5a, 5c, and 5d), the coefficients from this work, as well as those listed in Table 1 agree well with the in situ IWC data with differences as large as $\pm 40\%$. In contrast, for the comparison from 11 July

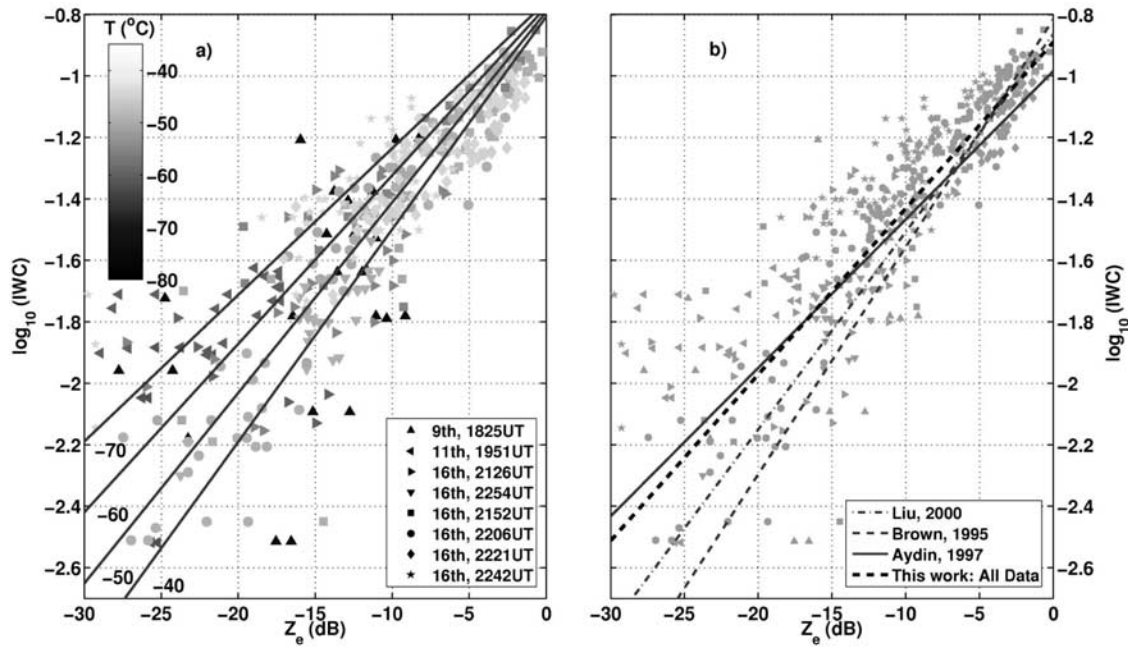


Figure 3. Scatter plots of Z_e (dB) from CRS versus $\log_{10}(\text{IWC})$ from HVTW for eight different flight segments. (a) Each flight segment is plotted as a different symbol according to the legend and shaded by temperature as given by the colorbar. Also shown are IWC- Z_e relationships using the coefficients of Protat *et al.* [2007] which are given as a function of temperature. Lines for -70 , -60 , -50 , and -40°C are shown from left to right. (b) Plot of all data from the eight flight segments as well as the least square fit to all the data shown as a black thick-dashed line. Also shown are fits using coefficients of Liu and Illingworth [2000], Brown and Illingworth [1995], and Aydin and Tang [1997] in the lighter shade of gray.

(Figures 4b and 5b), all the relationships underpredict the amount of ice by between 20 and 60%, with Protat *et al.* [2007] giving the best agreement. However, this can possibly be attributed to the predominance of small particles as this is the thinnest cirrus layer presented in this comparison. For the thick cirrus cases, all of which are from 16 July, the agreement between in situ and remote data vary between a few and 50% depending on which relationship is used. For the comparisons shown in Figures 4e and 5e the Brown and Illingworth [1995], Liu and Illingworth [2000], and coefficients from this work agree with the in situ IWC to within 20%. For the comparisons shown in Figures 4f and 5f the Protat *et al.* [2007] and coefficients from this work agree with the in situ IWC to within 20%. For the comparison shown in Figures 4g and 5g the Aydin and Tang [1997], Liu and Illingworth [2000], and coefficients from this work give the best agreement, and for the comparison shown in Figure 4h and 5h none of the parametrizations agree well over the

whole flight leg, with differences ranging from 10 to 50%. However, this is also the case with the worst spatial overlap with distances ranging between 1 and 2.5 km. The comparisons presented in Figures 3, 4, and 5 show that a single IWC- Z_e relationship is able to reproduce the IWC from in situ data to within a few to 20% for thicker cirrus and to 40% for thinner cirrus depending on the flight leg. The question that now must be addressed is whether this variability in agreement represents variability in the IWC- Z_e relationship or is due to sampling error.

4. Quantifying Sampling Error due to Inadequate Spatial Overlap

[26] In order to quantify the sampling errors associated with comparing measurements that are not collocated, synthetic clouds, of the type observed during CRYSTAL-FACE, are generated using DHARMA (a cloud resolving

Table 1. Parameters for IWC- Z_e relationships from several sources^a

Source	Cloud Type	Source of IWC/ Z_e	a	b
Sassen [1987]	ground measurements, precipitating ice crystals	size spectra/radar	0.12	0.696
Brown and Illingworth [1995]	north latitude frontal systems and tropical cirrus	in situ size spectra	0.153	0.74
Liu and Illingworth [2000]	north latitude frontal systems and tropical cirrus	in situ size spectra	0.137	0.643
Atlas <i>et al.</i> [1995]	midlatitude clouds	in situ size spectra	0.064	0.58
Aydin and Tang [1997]	hexagonal columns plates	modeled size spectra	0.104	0.483
Protat <i>et al.</i> [2007] ^b	midlatitude systems	in situ size spectra	0.162	0.62
This work	midlatitude anvil cirrus	in situ/radar	0.13	0.54

^aCoefficients a and b are least squares fits to $\text{IWC} = aZ_e^b$ where IWC is measured in g/m^3 and Z_e is measured in mm^6m^{-3} .

^bCoefficients are given at -50°C .

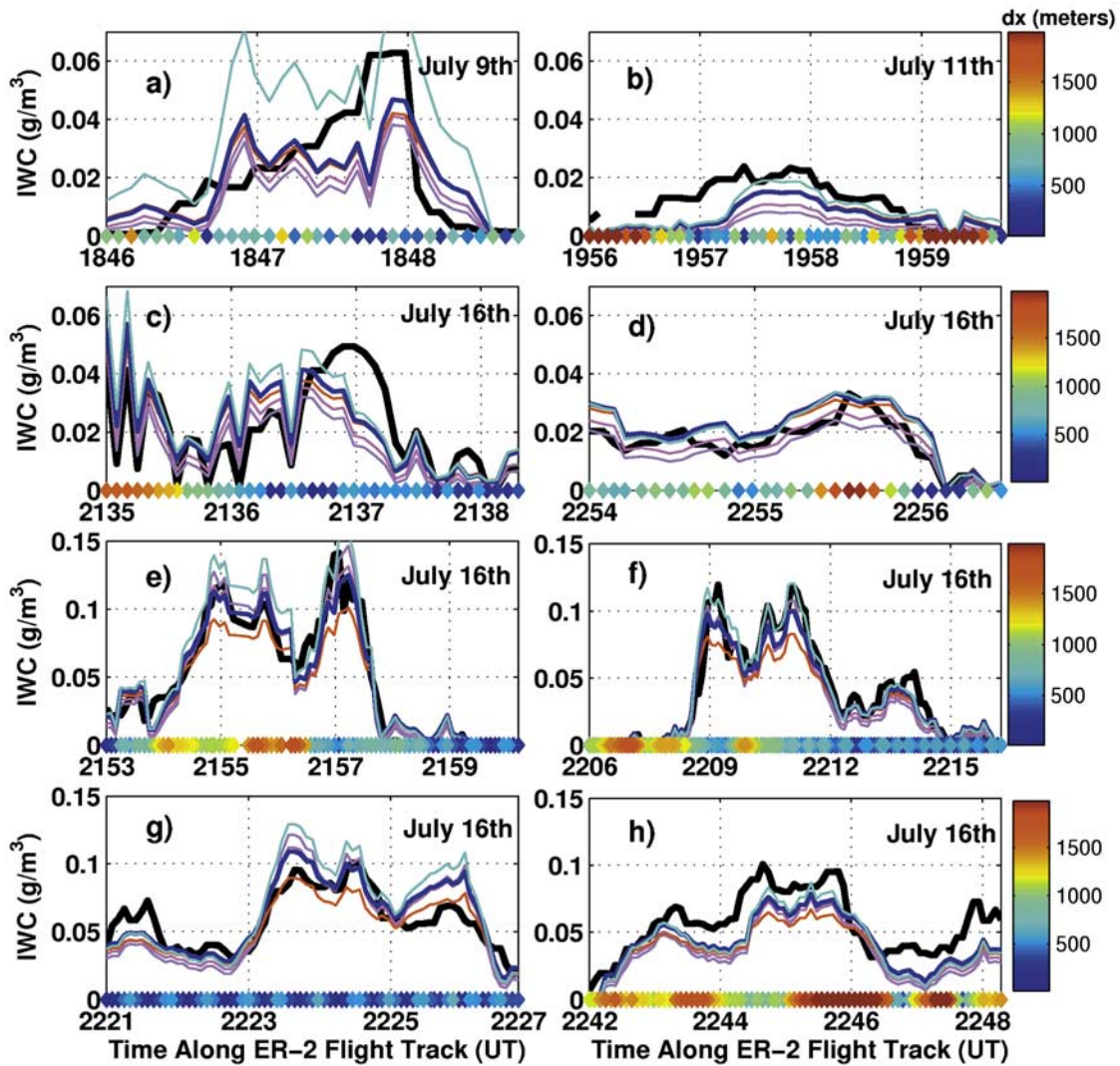


Figure 4. Eight plots represent all the comparisons that were made during CRYSTAL-FACE where the air parcels sampled by the WB-57 and ER-2 were within 2 km of each other. For each comparison the in situ IWC data are plotted in black and the derived IWC data using parameters obtained from this work are plotted in blue. Also shown are derived IWC data using the relationships described by *Brown and Illingworth* [1995], *Liu and Illingworth* [2000], *Protat et al.* [2007], and *Aydin and Tang* [1997] in purple, magenta, cyan, and red, respectively. Note that the y axis scale is different for the top four and bottom four plots.

microphysics model) [*Ackerman et al.*, 2004; *Fridlind et al.*, 2004; *Stevens et al.*, 2002]. The output from the model simulates the cirrus cloud inhomogeneities observed during CRYSTAL-FACE making it well suited for studying the sampling error between measurements that are not collocated. The results presented here use simulations of the cloud sampled by the WB-57 and ER-2 on 16 July. We use a simulation to evaluate sampling error in order to temporarily remove the uncertainties associated with the instruments or with deriving IWC from Z_e from the analysis. This means that any differences between two synthetic measurements from the simulation must be caused by sampling error resulting from insufficient overlap between the two measurements.

[27] To quantify how close two measurements must be to each other in order to ensure that the sampling error is less than or comparable to the instrument uncertainty, we

calculate the average error between measurements of IWC by two aircraft flying parallel to each other but separated by some distance. By using different transects through the simulated cloud at different altitudes the sampling error can be calculated for different spatial separations and different levels of cloud inhomogeneity. In Figure 6, IWC is plotted at a particular altitude within a cloud, in this case a simulation of the cloud system sampled by the WB-57 and ER-2 on 16 July 2002. The upper contour plot is a horizontal slice through the cloud at an altitude of 16.3 km, and the lower contour plot is at an altitude of 15.6 km. Both plots show contours of IWC in g/m^3 as indicated by the color bar to the right of each plot. The graphs below each contour plot show the fractional difference between two measurements separated by a distance of 0–10 km for each altitude, with the median value for each separation

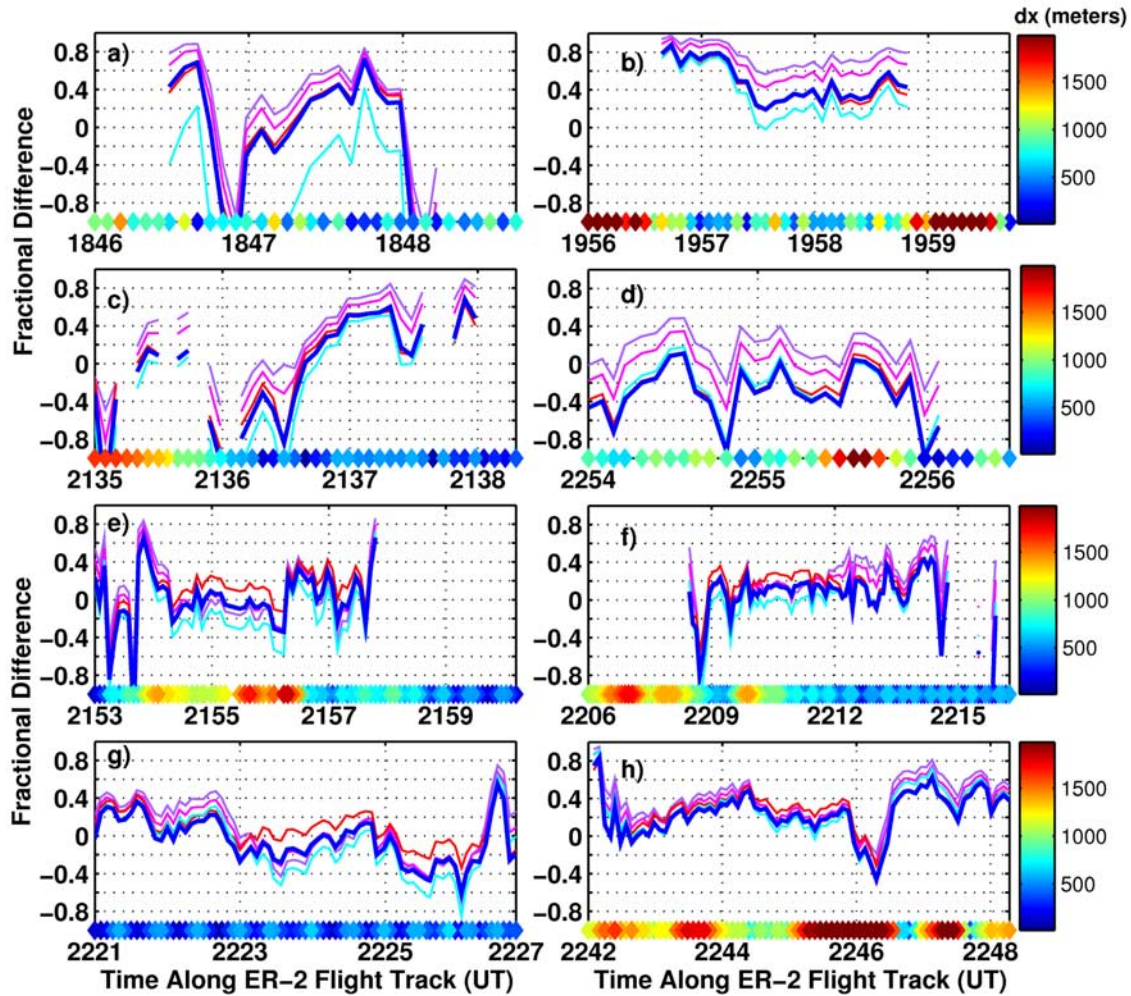


Figure 5. Comparisons that were made during CRYSTAL-FACE where the air parcels sampled by the WB-57 and ER-2 were within 2 km of each other. The data are plotted as the fractional difference between the in situ IWC data from HVTW and the derived IWC data. Differences from derived IWC data using parameters obtained from this work are plotted in blue. Also shown are differences from derived IWC data using the relationships described by *Brown and Illingworth* [1995], *Liu and Illingworth* [2000], *Protat et al.* [2007], and *Aydin and Tang* [1997] in purple, magenta, cyan, and red, respectively.

distance plotted as black squares. For the horizontal slice at 16.3 km the error caused by two aircraft sampling parcels that are separated by 1 km is 15% and by 2 km is 30%. For the horizontal slice at 15.6 km the error caused by two aircraft sampling parcels that are separated by 1 km is 10% and by 2 km is 20%. It is important to note that the level of inhomogeneities in the cloud have a large vertical dependence, and therefore the restrictions on the coordination of two aircraft may depend both on the type of cloud and location within a particular cloud. To reduce the necessity of coordinating two aircraft to be collocated horizontally to within 1–2 km, the in situ aircraft would ideally be sampling in the thicker parts of the cirrus.

5. Conclusions

[28] The comparisons between in situ IWC and remotely measured Z_e made during the CRYSTAL-FACE mission show a consistent IWC- Z_e relationship for the cirrus clouds sampled over Florida, within the uncertainty due to sam-

pling error. This was the first comparison in which both in situ IWC and remote measured Z_e were used, as previous studies relied on converting particle size spectra into IWC and Z_e . The agreement observed between in situ IWC and IWC derived from Z_e is approximately 20% when comparing in situ air parcels that were within 2 km of remotely measured air parcels. The best agreement came from using parameters either derived from the CRYSTAL-FACE mission or using parameters from *Liu and Illingworth* [2000]. In two cases, using the parameters from *Protat et al.* [2007], which are based on temperature, improved the agreement. Previous comparisons based on particle size distributions found errors ranging from 50% to –30% in IWC for a given Z_e [*Liu and Illingworth*, 2000] to 210% to –70% in IWC for a given Z_e [*Protat et al.*, 2007].

[29] Because of the requirement that the air parcels sampled by in situ and remote instruments be collocated to within 2 km, during the CRYSTAL-FACE mission only 37 min out of more than 70 h of flight time are usable for direct comparisons. This restriction, on which comparisons

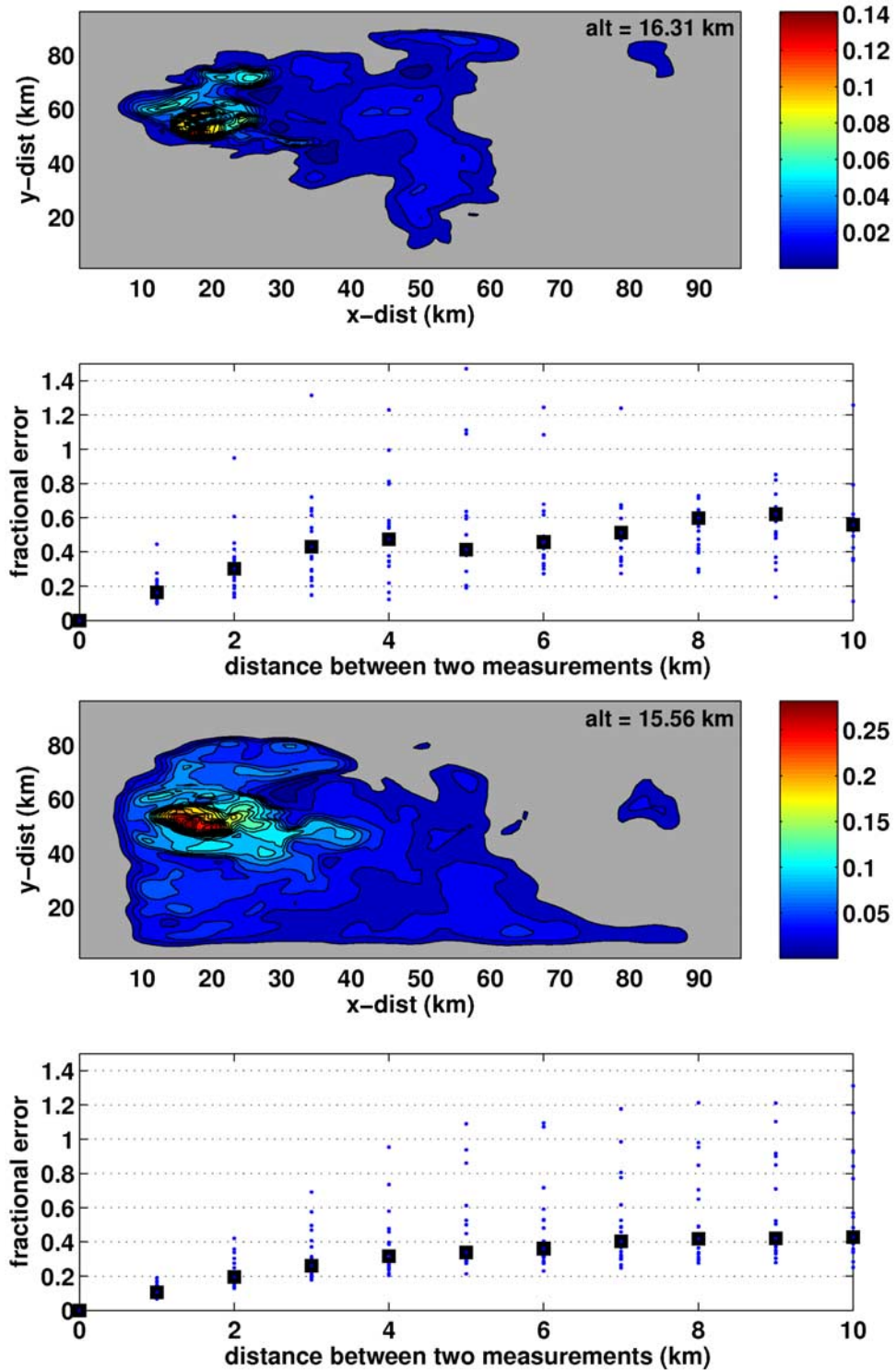


Figure 6. Contour plots show IWC (g/m^3) from the cloud model at altitudes of 16.3 and 15.6 km. The graphs show the fractional error between two measurements of the same cloud as the distance between the measurements increases from 0 to 10 km. The blue points are the average fractional error calculated between two random trajectories through the cloud separated by a distance of 0 to 10 km. The black squares are the median values at each distance for 10 random trajectories.

can be used, is important since once the sampling error becomes larger than the instrument uncertainty it is not possible to distinguish variability in the IWC- Z_e relationship, because of microphysical differences between the

cloud samples, from sampling error. Most of the flight legs presented in this work were made on 16 July, which means that the relationship derived has only been validated for a single cloud. In order to both derive IWC- Z_e relationships

for different types of clouds and to validate IWC retrieval algorithms for either airborne- or satellite-based radar the frequency of valid comparison opportunities for a flight mission must be increased.

[30] To quantify the uncertainty associated with sampling error, we have used the DHARMA model to simulate the cirrus sampled during CRYSTAL-FACE. The model predicts that a sampling error of 20–30% for air parcels separated by 2 km would be expected for the cirrus encountered during CRYSTAL-FACE. This means that the discrepancies between in situ IWC and IWC derived from Z_e during CRYSTAL-FACE are consistent with the expected sampling error because of the measurements not being collocated and do not indicate that several IWC- Z_e relationships are necessary to explain the clouds sampled during CRYSTAL-FACE. The maximum allowable separation distance will vary for different clouds, since the sampling error depends on cloud inhomogeneities.

[31] While the results from the CRYSTAL-FACE mission seem promising, a much larger data set is needed in order to evaluate how well a single IWC- Z_e relationship describes similar types of clouds. In order to increase the quantity of usable observations, specific missions, or flight days within a mission, will have to be devoted to coordinated flights. The flight of 16 July was a perfect example that this is feasible. However, it requires that the two aircraft make multiple along-wind transects through a single cloud. During CRYSTAL-FACE this was only done once. For future missions, three or four flights during the campaign could be devoted to this type of validation. Given the flight time of the WB-57 and ER-2, only a small percentage of a single cloud can be sampled during a flight. Longer flight times, perhaps using uninhabited aerial vehicles, may be necessary to improve the validation of A-Train satellites. Given the importance of clouds in the climate system and the importance of having quantitative measurements from A-Train satellites, aircraft campaigns will have to be able to provide large quantities of in situ data with sufficient overlap in order to quantitatively validate remote sensing instruments.

[32] **Acknowledgments.** The authors gratefully acknowledge the hard work of the WB-57 and ER-2 pilots and crew during the CRYSTAL-FACE mission. We also thank Thomas Hanisco for his insightful comments during the preparation of this manuscript. Support from NASA grants NAG5-11548, NAG5-115487, NAG5-8779, and NAG1-01095 are gratefully acknowledged.

References

- Ackerman, A. S., M. P. Kirkpatrick, D. E. Stevens, and O. B. Toon (2004), The impact of humidity above stratiform clouds on indirect aerosol climate forcing, *Nature*, **432**, 1014–1017.
- Atlas, D., S. Y. Matrosov, A. J. Heymsfield, M.-D. Chou, and D. B. Wolf (1995), Radar and radiation properties of ice clouds, *J. Appl. Meteorol.*, **34**, 2329–2345.
- Aydin, K., and C. X. Tang (1997), Relationships between IWC and polarimetric radar measurands at 94 and 220 GHz for hexagonal columns and plates, *J. Atmos. Oceanic Technol.*, **14**, 1055–1063.
- Baran, A. J. (2005), The dependence of cirrus infrared radiative properties on ice crystal geometry and shape of the size-distribution function, *Q. J. R. Meteorol. Soc.*, **131**(607), 1129–1142.
- Brown, P. R. A., and A. J. Illingworth (1995), The role of spaceborne millimeter-wave radar in the global monitoring of ice cloud, *J. Appl. Meteorol.*, **34**, 2346–2366.
- Buschmann, N., G. M. McFarquhar, and A. J. Heymsfield (2002), Effects of observed horizontal inhomogeneities within cirrus clouds on solar radiative transfer, *J. Geophys. Res.*, **107**(D20), 4445, doi:10.1029/2001JD001273.
- Davis, S. M., L. M. Avallone, E. M. Weinstock, C. H. Twohy, J. B. Smith, and G. L. Kok (2007), Comparisons of in situ measurements of cirrus cloud ice water content, *J. Geophys. Res.*, **112**, D10212, doi:10.1029/2006JD008214.
- Donovan, D. P. (2003), Ice-cloud effective particle size parameterization based on combined lidar, radar reflectivity, and mean Doppler velocity measurements, *J. Geophys. Res.*, **108**(D18), 4573, doi:10.1029/2003JD003469.
- Fridlind, A. M., et al. (2004), Evidence for the predominance of mid-tropospheric aerosols as subtropical anvil nuclei, *Science*, **304**, 718–722.
- Gultepe, I., G. A. Isaac, and K. B. Strawbridge (2001), Variability of cloud microphysical and optical parameters obtained from aircraft and satellite remote sensing measurements during race, *Int. J. Climatol.*, **21**, 507–525.
- Jensen, E., D. Starr, and O. B. Toon (2004), Mission investigates tropical cirrus clouds, *Eos Trans. AGU*, **84**(5), 45–50.
- Li, L. H., G. M. Heymsfield, P. E. Racette, L. Tian, and E. Zenker (2004), A 94-GHz cloud radar system on a NASA high-altitude ER-2 aircraft, *J. Atmos. Oceanic Technol.*, **21**, 1378–1388.
- Liao, L., and K. Sassen (1994), Investigation of relationships between Ka-band radar reflectivity and ice and liquid water contents, *Atmos. Res.*, **34**, 231–248.
- Liu, C. L., and A. J. Illingworth (2000), Toward more accurate retrievals of ice water content from radar measurements of clouds, *J. Appl. Meteorol.*, **39**, 1130–1146.
- Nasiri, S. L., B. A. Baum, A. J. Heymsfield, P. Yang, M. R. Poellot, D. P. Kratz, and Y. X. Hu (2002), The development of midlatitude cirrus models for MODIS using FIRE-I, FIRE-II, and ARM in situ data, *J. Appl. Meteorol.*, **41**, 197–217.
- Norris, J. R. (2000), What can cloud observations tell us about climate variability?, *Space Sci. Rev.*, **94**, 375–380.
- Pawlowska, H., et al. (2000), Microphysical and radiative properties of stratocumulus clouds: The EUCREX mission 206 case study, *Atmos. Res.*, **55**, 85–102.
- Protat, A., J. Delanoe, D. Bouniol, A. J. Heymsfield, A. Bansemer, and P. Brown (2007), Evaluation of ice water content retrievals from cloud radar reflectivity and temperature using a large airborne in situ microphysical database, *J. Appl. Meteorol. Climatol.*, **46**, 557–572.
- Sassen, K. (1987), Ice cloud content from radar reflectivity, *J. Clim. Appl. Meteorol.*, **26**, 1050–1053.
- Sassen, K., Z. Wang, V. I. Khvorostyanov, G. L. Stephens, and A. Benedetti (2002), Cirrus cloud ice water content radar algorithm evaluation using an explicit cloud microphysical model, *J. Appl. Meteorol.*, **41**, 620–628.
- Scott, S. G., T. P. Bui, K. R. Chan, and S. W. Bowen (1990), The meteorological measurement system on the NASA ER-2 aircraft, *J. Atmos. Oceanic Technol.*, **7**(4), 525–540.
- Stephens, G. L. (2005), Cloud feedbacks in the climate system: A critical review, *J. Clim.*, **18**, 237–273.
- Stephens, G. L., et al. (2002), The CloudSat mission and the A-train: A new dimension of space-based observations of clouds and precipitation, *Bull. Am. Meteorol. Soc.*, **83**, 1771–1790.
- Stevens, D. E., A. S. Ackerman, and C. S. Bretherton (2002), Effect of domain size and numerical resolution on the simulation of shallow cumulus convection, *J. Atmos. Sci.*, **59**, 3285–3301.
- Wang, Z., and K. Sassen (2002a), Cirrus cloud microphysical property retrieval using lidar and radar measurements: part I: Algorithm description and comparison with in situ data, *J. Appl. Meteorol.*, **41**, 218–229.
- Wang, Z., and K. Sassen (2002b), Cirrus cloud microphysical property retrieval using lidar and radar measurements: part II: Midlatitude cirrus microphysical and radiative properties, *J. Atmos. Sci.*, **59**, 2291–2302.
- Weinstock, E. M., et al. (2006a), Measurements of the total water content of cirrus clouds: part I: Instrument details and calibration, *J. Atmos. Oceanic Technol.*, **23**(11), 1397–1409.
- Weinstock, E. M., J. B. Smith, D. Sayres, J. V. Pittman, N. Allen, and J. G. Anderson (2006b), Measurements of the total water content of cirrus clouds: part II: Instrument performance and validation, *J. Atmos. Oceanic Technol.*, **23**(11), 1410–1421.

A. S. Ackerman and A. M. Fridlind, NASA Goddard Institute for Space Studies, 2880 Broadway Street, New York, NY 10025, USA.

J. G. Anderson, J. V. Pittman, D. S. Sayres, J. B. Smith, and E. M. Weinstock, Department of Earth and Planetary Sciences, Harvard University, 20 Oxford Street, Cambridge, MA 02138, USA. (sayres@huarp.harvard.edu)

G. Heymsfield, Goddard Space Flight Center, NASA, 8800 Greenbelt Road, Greenbelt, MD 20771, USA.

L. Li, University of Maryland Baltimore County, 1000 Hilltop Circle, Baltimore, MD 21250, USA.